FINITE ELEMENT ANALYSIS (FEA) IMPLEMENTATION OF THERMAL BARRIER COATING (TBC) LIFETIME PREDICTION METHODS

by

Hassan Mohamed

B. S. in Engineering, Massachusetts Institute of Technology, 2009

Submitted to the Graduate Faculty of

Swanson School of Engineering in partial fulfillment

of the requirements for the degree of

Master of Science

University of Pittsburgh

2013

UNIVERSITY OF PITTSBURGH

SWANSON SCHOOL OF ENGINEERING

This thesis was presented

by

Hassan Mohamed

It was defended on

December 20th, 2012

and approved by

William S. Slaughter, PhD, Associate Professor, Department of Mechanical Engineering and Materials Science

Anne M. Robertson, PhD, Associate Professor, Department of Mechanical Engineering and Materials Science

Patrick Smolinski, PhD, Associate Professor, Department of Mechanical Engineering and Materials Science

Thesis Advisor: William S. Slaughter, PhD, Associate Professor, Department of Mechanical Engineering and Materials Science

FINITE ELEMENT ANALYSIS (FEA) IMPLEMENTATION OF THERMAL BARRIER COATING (TBC) LIFETIME PREDICTION METHODS

Hassan Mohamed, M.S.

University of Pittsburgh, 2013

Thermal Barrier Coatings (TBC) is one of the most important insulation components of an advanced turbine. It is expected to operate at temperature conditions as high as 1760ºC. The main objective of this work is to investigate four available methods in predicting the lifespan of the TBC layer and its practicality in finite element analysis (FEA) computation. The four methods discussed are TGO Thickness Calculation, Elasticity and Creep Effect Analysis, A Coupled Oxidation Constitutive Approach and Fracture Mechanics Method. The predicted results obtained are compared with experimental data provided by Limarga [10]. The implementations of TGO Thickness Calculation as well as Elasticity and Creep Effect Analysis in finite element computation have shown a promising result such as local von Mises stress distribution on each layer in TBC (top coat, TGO and bond coat). This simulation result can provide a good comparison data for future experimental work.

TABLE OF CONTENTS

LIST OF TABLES

LIST OF FIGURES

NOMENCLATURE

α	Thermal expansion coefficient, K^{-1}
A_0	Proportionality constant, $\mu m\text{-}s^{-m}$ ($1\ \mu m\text{-}s^{-m}$)
E	Young's Modulus, $N \cdot m^{-2}$
D	Damage parameter based on elastic failure theories
e_V^T	Mean local dilatational strain due to transformation of f_2
f_1^{ini}	Initial oxidation resistant phase volume fraction
f_2^{ini}	Initial oxidation-prone phase volume fraction
f_2	Unoxidized fraction of phase 2 f_2^{ini} volume fraction
f_3	New metallic phase of volume fraction
f_{ox}	Primary oxide volume fraction
h	Thickness, m
h_{ox}	TGO Thickness due to external oxidation, m
h_{in}	TGO Thickness due to internal oxidation, m
k	Thermal conductivity, $Wm^{-1}K^{-1}$
R	Universal gas constant
r_{ox}	Final volume fraction of the oxide in the oxidized Phase 2
T	Temperature, K
t	Time, s

v	Poisson ratio
θ	Absolute temperature, K
θ_R	Reference temperature (2424 K)
m	Growth exponent (0.332)

ACKNOWLEDGEMENTS

I would like to thank my advisor, Dr. William S. Slaughter, for his patience and guidance throughout the course of my research, and for giving me the exceptional support and opportunity to continue my graduate studies as well as providing me with an outstanding atmosphere for research.

I would also like to thank Dr. Ventzi Karaivanov, who greatly contributed to my growth as a researcher and to better understand the research. I am grateful to the members of my thesis defense committee, Dr. Anne M. Robertson and Dr. Patrick Smolinski.

My deepest gratitude to all faculty and students at the Department of Mechanical Engineering and Materials Science.

Last but not least to my wife Fazliyana Zaabar and our families who continuously provide their supports and love.

1.0 INTRODUCTION

In the next generation of power plant technology, both oxy fuel and hydrogen fuel may be utilized as the substitute for current combustion technology. Both future technologies in power generation may enable advanced turbines to operate more efficiently but at a significantly higher temperature condition compared to today's current power plant condition. Such advanced turbines with oxy fuel or hydrogen fuel operate approximately up to 1760 °C, while the current coal-fueled power plants operate at a temperature only up to 900 °C. Due to the high temperature operating condition, these technologies may require a change in its material design. One of the most important components in a power plant that will be affected is the turbine blades, since the availability of the power plant mainly depends on the lifespan of the blades.

The materials used to build turbine blades will likely require high temperature resistance in order to withstand such conditions. One of the potential means of protecting the blades is by applying a thermal barrier coating (TBC) on their surfaces. Such a coating may help to protect the nickel based super alloy blade from hot gas steam. Nevertheless, the TBC layer is also in contact with both the increasing operating metal temperature and the kinetics of the base material, each of which gradually degrades TBC durability, exposing itself to damage failures such as undulation, spallation, and cracking.

Thus this project will study the thermomechanics of the TBC layer in order to predict its lifespan before failure occurs. Several approaches in modeling the TBC lifetime have been

identified and applied in a finite element computer simulation. This paper intends to discuss four damage modeling approaches: TGO thickness calculation, elasticity and creep effect of TBC, a coupled oxidation-constitutive approach and fracture mechanics approach. Of the methods, only two techniques, TGO thickness calculation and elasticity and creep effect of TBC, are employed in the finite element analysis.

2.0 BACKGROUND

Thermal Barrier Coating is widely used in aircraft and industrial gas turbine engines. Commercial manufactured TBC system consists of two layers, a ceramic top coat and underlying metallic bond coat. The top coat is a composition of yttria-stabilized zirconia (YSZ) that can be composed by air plasma spraying (APS) or electron-beam physical vapor deposition (EB-PVD). The top coat has low thermal conductivity, high oxygen permeability, and relatively high coefficient of thermal expansion. Due to its low thermal conductivity characteristic, its main function is to provide a thermal insulation on the turbine blades surface from the hot gas steam.

The metallic bond coat is normally made of MCrAlY overlay or a platinum-modified diffusion aluminide (β-NiAl-Pt). The work on this study mainly focuses on APS TBC system with MCrAlY bond coat. Since the top coat has very high oxygen permeability while the bond coat is rich with aluminum properties, both layers inevitably form a protective, thermally grown oxide (TGO) scale of α-Al_2O_3 during thermal operation. This TGO scale provides strong attachment between the YSZ top layer and metallic bond coat layer.

All the layers existed in TBC system equip the TBC system with the capability of thermal insulation as well as oxidation resistant to protect nickel-based super alloy metal below it. TBC systems are able to create high temperature drop from about 140°C up to 250°C with cooling systems, which subsequently reduces the metal operating temperature [1]. Nevertheless, the TGO is gradually thickening over the period of time during high temperature exposure.

Hence, the crucial failures that associate with the TBC system are typically spallation and cracking of the thickening thermal growth oxidation (TGO) scale. Majority of the reviewed papers, then, agree that thermal growth oxidation (TGO) layer that is formed due to bond coat oxidation and interdiffusion with metallic bond coat strongly contributes to such failures. The following section will discuss the constitutes of the TBC systems in more details.

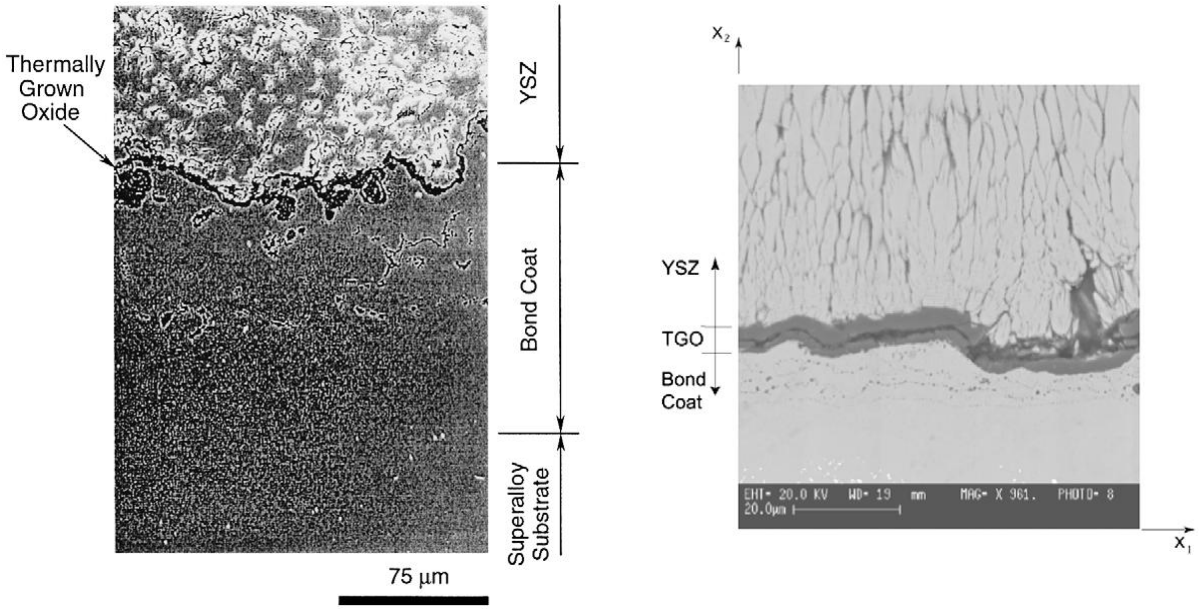

Figure 1: a) Microstructure of a typical plasma sprayed thermal barrier coating after 500 hours oxidation at 950ºC (Busso [3]). b) A typical microstructure of an EB-PVD TBC system after 700 hours at 1000ºC (Busso[6]).

2.1 CERAMIC TOP COAT LAYER

The layer is made of Y_2O_3 (yttria) stabilized ZrO_2 (zirconia). Y_2O_3 is found to be empirically suitable to stabilize ZrO_2 compared to other different oxides (MgO, CeO_2, Sc_2O_3, In_2O_3, CaO) because of its structure that can exist in three different polymorphs such as monoclinic,

tetragonal, and cubic. The polymorphs structures of Y_2O_3 vary according to the composition and the temperature condition. For example, by adding 7 to 8 weight % which is around 4 to 4.5 mol% of Y_2O_3 into zirconia solid solution, Y_2O_3 can stabilizes ZrO_2 tetragonal crystal structure especially metastable tetragonal-prime structure (t'-YSZ) . This t' phase is considered as the most desirable and stable phase for TBC applications because it does not undergo martensitic transformation on cooling even after multiple thermal cycles. As a result, Y_2O_3 has been found as a consistent stabilizer for zirconia solid solution, subsequently makes yttria-stabilized zirconia YSZ as the most applicable composition for thermal barrier coating applications. Nevertheless, the detailed reason is not yet being explained and remains one of the important aspects of ongoing research.

One of the most important material properties of the YSZ top coat is its low thermal conductivity, k at high temperature, which is around 2.3 $Wm^{-1}K^{-1}$ at 1000°C. The thermal conductivity is low because of the high distribution of point defects such as oxygen vacancies and substitutional solute atoms that can scatter heat-conducting phonons (lattice waves). Heat is transferred by lattice vibrations and radiation in electric insulators such as ZrO_2. Therefore, as more phonons and photons being scattered by the point defects in the lattice structure of the ZrO_2 ceramic, thermal conductivity can be efficiently reduced.

In addition, YSZ has a high thermal-expansion coefficient, α, which is around 11×10^{-6} $°C^{-1}$. It is comparable to the metallic bond coat thermal expansion coefficient ($14 \times 10°C^{-1}$), and thus it can lessen the thermal expansion mismatch stress between the metallic bond coat and ceramic top coat. YSZ ceramic top coat is also resistant to erosion and external impact because of its high hardness property, which is approximately 14 GPa. The density of YSZ layer is relatively low just about 6.4 $Mg{\cdot}m^{-3}$, yet it is useful for parasitic weight consideration in

moving engine components. Another crucial aspect of the YSZ top coat is its high melting point. This ceramic layer is resistant to elevated temperature up to approximately ~2700 °C which makes YSZ as the most significant component in TBC system. There are two most important types of YSZ top layer coating depositions, air plasma spraying (APS) and electric-beam physical vapor deposition (EB-PVD). This paper, however, focuses on the APS TBC system life damage simulation since it is commonly used in power plant turbines.

2.1.1 ELECTRON-BEAM PHYSICAL-VAPOR DEPOSITED TBC

The EB-PVD top coat is approximately 125 μm thick. The microstructural features of the top coat consist of a thin region on polycrystalline YSZ with equiaxed grains near the ceramic/metal interface. The EB-PVD top coat is deposited into columns of YSZ grains with diameter of 2 to 10μm. The columnar YSZ grains grow outwardly from the equiaxed-grain region to the top surface. Within the columnar YSZ grains, there are nanometer-scale porosity, and channels, normal to the ceramic/metal interface that separates the YSZ columns. This columnar grains separation can disconnect at elevated temperature, alleviating the effect from the stress that rises from thermal expansion mismatch. This behavior is known as "strain tolerance". The EB-PVD top coat is smoother than APS deposition. Plus, it is more durable and expensive compared to APS case. Thus, it is typically used in the most harsh temperature condition like in aircraft engines.

2.1.2 AIR-PLASMA-SPRAYED TBC

Unlike EB-PVD top coat, a typical APS top coat is slightly thicker than EB-PVD top coat with a thickness of 300 μm to 600μm. The APS top coat structure consists of "splat" grain morphology which each "splat" has 1 to 5 μm thickness and about 200 to 400 μm diameter. Besides inter-"splat" boundaries, there are also cracks that exists parallel to the ceramic/metal, creating 15 to 25 vol% porosity within the APS TBC that contributes to low thermal conductivity and low elastic modulus of the system.

The weakness of the APS TBC is the undulating nature of the ceramic/metal interface that is actually needed in sticking together the top coat and the metal bond coat. This nature is found to be the cause of the undulation failures due to the stress it creates. The commercial production cost of APS system is relatively low. Hence, it becomes a preferable choice for applications that operate in slightly lower temperature condition and fewer thermal cycles such as in conventional power plant gas-turbine engines. However, the thermal-cycle life of APS top coat is usually shorter than EB-PVD TBC's live because of the growing microstructural defects parallel to the interface and also the roughness of the interface within the APS TBC. Table 1 below shows the material properties comparison of APS and EB-PVD TC systems at a room temperature.

Table 1: Room temperature properties of YSZ top coats [1].

Property	***Deposition Method***	
	APS	***EB-PVD***
Thermal Conductivity (Wm^{-1} K^{-1})	1.5-1.9	0.8-1.1
Surface Roughness, μm	0.5-1	4-10
Adhesion Strength, (MPa)	400	20-40
Young's Modulus (GPa)	90	200
Erosion rate (normalized to PVD)	1	7

2.2 BOND COAT LAYER

Metallic coatings for super alloys are typically NiCrAlY type which contains 15 to 25 weight % Chromium (Cr), 10-15% Aluminum (Al), and 0.2-0.5% Yttrium (Y) and β-NiAl phase. The bond coat has a typical thickness of 40 to 100μm, depending on the deposition method. Similar to YSZ top coat deposition, the metallic coatings are commonly deposited by using EB-PVD method or low pressure plasma spraying (LPPS) in today's gas turbines applications. The LPPS process is relatively cheaper than EB-PVD and becomes a favorable selection. Nonetheless, EB-PVD has a quality advantage over LPPS.

The key physical property of the bond coat is its oxidation behavior. The metallic bond coat should be able to oxidize in order to form a nonporous and adherent oxide layer, which is called thermal growth oxidation layer. Therefore, the composition, microstructure, and surface condition of metallic bond coat is considered important to study in order to observe its influence on a TGO formation. The function of TGO layer is discussed in more detail in section 2.3 **Thermal Growth Oxidation layer.** Table 2 below shows the mechanical properties of NiCrAlY bond coat at room temperature.

Table 2: Mechanical properties of NiCrAlY bond coat at room temperature.

Properties	***Values***
Young's Modulus, E (GPa)	200
Poisson Ratio	0.3
Thermal Expansion Coefficient, α ($\times 10^{-6}$, $^{o}C^{-1}$)	12.3
Material Strength, σ_Y (MPa)	226

2.3 THERMAL GROWTH OXIDATION LAYER

The thermal growth oxidation layer α-Al_2O_3 is formed during the thermal operation and the oxidation of the metallic bond coat. The Al in bond coat slowly depletes and thickens the TGO layer. This TGO layer is considered the most crucial layer in the TBC system. Its growth during the thermal operation is responsible for the spallation failure of TBC system in many ways. One of the causes is from the stresses created inside the TGO. As the TGO thickens, the volume expands and at the same time the volume expansion is restrained by the top coat and bond coat layers. The restriction creates compressive "growth" stress (< 1 GPa) within the TGO.

Another source of stress is from thermal expansion mismatch between the TGO and the bond coat during cooling process. This thermal compressive residual stress is quite high as it can reach a maximum stress value that is about 2 to 6 GPa when the TGO is cooled down to ambient temperature. All these internal stresses can initiate and aggravate the development of micro cracks inside the TGO during thermal operation. As a result, total damage failure due to TBC spallation will occur from micro cracks coalescence. Thus, one way that can be used to predict the damage failure of TBC is by investigating the stresses created inside the TGO layer. Table 3 below shows the mechanical properties of TGO layer at room temperature.

Table 3: Mechanical properties of TGO layer at room temperature**.**

Properties	***Values***
Young's Modulus, E (GPa)	400
Poisson Ratio	0.18
Thermal Expansion Coefficient, α ($\times 10^{-6}$, $^{o}C^{-1}$)	8
Material Strength, σ_Y (MPa)	97

3.0 METHODS

Four methods that are used to predict the life span of the TBC system before it fails are:

1) TGO Thickness Calculation,

2) Creep Effect and Elasticity Analysis,

2) Coupled Oxidation Constitutive Approach, and

3) Fracture Mechanics.

All these methods are discussed except for Coupled Oxidation Constitutive Approach and Fracture Mechanics, both of which will not be analyzed using computer simulation because of modeling difficulty as is explained later.

3.1 TGO THICKNESS CALCULATION

This method is based on the calculation of the thickness of TGO formed during the oxidation and interdiffusion processes between the top coat layer and the bond coat layer. Most reviewed papers, [1] to [11], are in agreement that the thickening of the TGO layer being formed increases the tendency of cracking and spallation of the whole TBC system as its growth causes progressive aluminum depletion from the metallic bond coat. A critical thickness is then defined as the thickness of which the TBC layers completely spalls from the metal surface. In Busso's

model [4], the TGO thickness is calculated as a function of operating temperature as shown below.

$$h = \text{-}A_0 t^q \exp\left(\frac{Q_0}{R}\left(\frac{1}{\theta_R} - \frac{1}{\theta_{max}}\right)\right) \quad (1)$$

In a later experimentation by Echsler [2], the TGO thickness calculation is separated into an outward oxidation and an inward oxidation of the TGO layer as shown in the equations (2) and (3) respectively,

$$h_{ox}(t,T) = \text{-}K_n\,(\mathrm{T})\left(\frac{t}{t_0}\right)^{\mathrm{n}}, \quad (2)$$

$$h_{in}(t,T) = \text{-}B_n\,(\mathrm{T})\left(\frac{t}{t_0}\right)^{\mathrm{m}}. \quad (3)$$

The values for variables in Echsler's and Busso's equations (1), (2) and (3) are listed in references [2] and [4]. We decide to implement equations (1) and (2) to show the applicability of this method in finite element computation because the equations are dimensionally correct and straightforward to use on a finite element model.

However, there is no conclusive agreement between the studies on the critical thickness of the TGO scale. In Busso's paper [4] it is reported that the critical thickness is as low as 10 μm, while Echsler reported the thickness before failure at 12 μm. Furthermore, the critical TGO thickness typically varies depending on the type of application and operating condition. As a result, the TGO thickness calculation becomes a less favorable TBC lifetime prediction method to satisfy all operating conditions.

3.2 ELASTICITY AND CREEP EFFECT ANALYSIS

The thermal stress distribution of the coating layers operating in high temperature conditions can be studied by performing finite element computation. During the extreme operating temperature, creep damage is considered as one of the main contributors to the presence of stress and TBC failure. Hence, the creep behavior of all the layers - top coat (YSZ), TGO and bond coat (NiCoCrAlY) - are analyzed by using a Norton power-law equation as shown below,

$$\dot{\varepsilon} = A\sigma^{n}\mathrm{e}^{(-\frac{\mathrm{Q}}{\mathrm{RT}})} \tag{5}$$

The values for the creep properties *A*, *Q* and *n* for each layer are listed in Table 4 below

Table 4: Creep properties for top coat (YSZ), TGO and bond coat (NiCoCrAlY) layers.

Material	***A*** ***(s^{-1} MPa^{-n})***	***Q*** ***(kJ/mol)***	***n***
YSZ	10^{10}	625	4
TGO	6.8×10^{3}	424	1
NiCoCrAlY	10^{12}	500	3

The analysis mainly focuses on the elasticity effect of the layers. The material properties of the layers at different temperatures are listed in Table 5. All these values will be utilized in the computation of thermal stress distribution within the coating layer.

Table 5: Material properties of TBC layers used in finite element analysis [11].

Material	*T (°C)*	*E (GPa)*	*v*	*Yield Strength (MPa)*	*Density (kg/m^3)*	*CTE (ppm/ °C)*	*Thermal conductivity (W/mK)*	*Specific Heat (J/kg K)*
NiCrAlY	800	117	0.3	191	7320	16.30		
	900	100		92		16.94	24	674
	1000	74		52		17.51		
	1100	41				17.99	34	712
TGO	25	360	0.25		3970	8.00	20.00	790
	1000			100				
	1300			100				
YSZ	25	50	0.25		5100	10.00	0.70	479
	500					9.64	0.70	445
	1000					10.34	0.70	445

In this finite element computation, several assumptions are made to simplify the simulation process. Firstly, all interfaces such as top coat/TGO, TGO/bond coat and bond coat/super alloy are assumed to have a perfect bonding. In addition, the interfaces are assumed to be flat, neglecting the effects of the grain and roughness between the surfaces. Another assumption made is that the stress relaxation due to cracking is not taken into consideration.

Additionally, we assume the top coat, bond coat and TGO layers have isotropic material properties. However, this assumption is not entirely correct because the ceramic top coat for example, has a "splat" shape and the TGO layer has a unique shape as TGO depends on uncontrolled oxidation process. Hence, the material properties of each layer may significantly depend on directions. Nevertheless, due to limited information obtained on material properties of all the layers, we decide to assume their material properties to be isotropic for the present.

To perform the finite element simulation, the primary software used in this work is ANSYS. The finite element analysis first investigates the thermal stress on a small block element that only consists of the three layers, YSZ, TGO and NiCoCrAly with a uniform high ambient temperature as the boundary condition. This will open up possibilities of more sophisticated 3D

models of turbine blades with heat convection as a boundary condition. The result of the simulation is able to give a better representation of the thermal stress distribution within the coating. The stress distribution will be used to evaluate the TBC failure based on the failure criteria that we have defined as the ratio of local stress, σ_{local} to failure stress, σ_f, which is the material strength of the coating.

3.3 A COUPLED OXIDATION CONSTITUTIVE APPROACH

A coupled oxidation constitutive approach is a continuum mechanics-based mechanistic study that takes into account the effects of local stresses induced by oxidation, sintering process and thermomechanical loading on the overall APS-TBC damage evaluation. This method is suggested to explain the effect of phase transformations caused by local external and internal oxidation process through a multi-phase solid on the constitutive behavior of bond coat such as the local volumetric expansion of the new formed oxide layer. By using finite element analysis on a unit cell of a TBC layer, the stress distribution due to internal and external oxidation is observed. The steps of this method consist of:

1. Finding the value of an applicable stress measure, such as the maximum principal stress σ_{MPS} or the normal traction stress σ_{NT} acting on the interface that drives the crack nucleation and propagation.

2. Failure occurs when the stress measure reaches the failure stress σ_f (a TBC material property).

3.3.1 OXIDATION OF TWO PHASE METALLIC SYSTEM

The microstructural changes inside the oxidized multiphase Ni-base metallic bond coat interlayer needs to be investigated in order to resolve the limiting stress condition for micro crack initiation in the TGO layer.

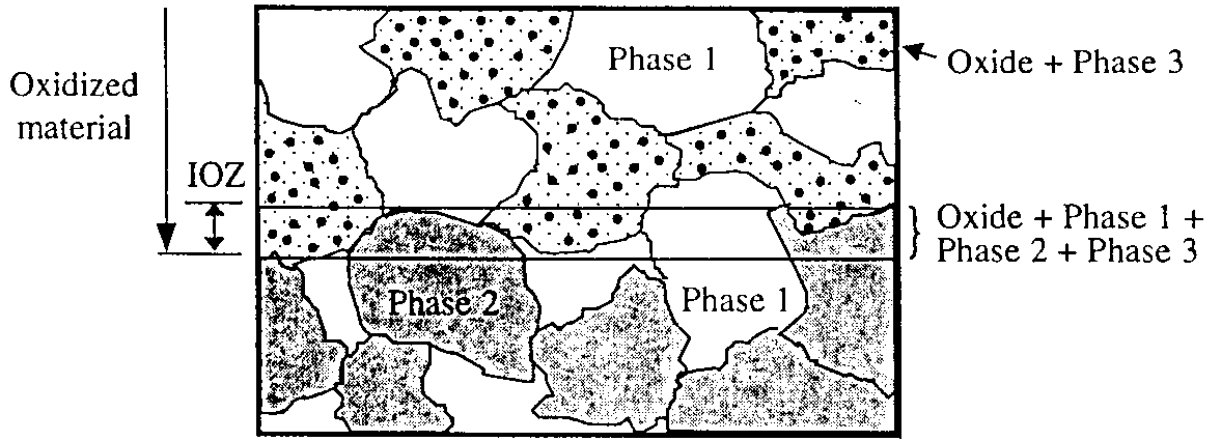

Figure 2: Oxidation process on the multiphase Ni-metallic bond coat [7].

To formulate oxidation process, two solid phase system consisted of oxidation resistant phase, f_1^{ini} and an oxidation-prone phase, f_2^{ini} are considered as phases that existed in the initial volume fractions which are also assumed to be isotropically homogenous grain aggregates. When the oxidation process starts, a new layer is formed beneath the ceramic/metal interface which is recognized as internal oxidation zone (IOZ) where it consists of four different phases which are oxidation resistant phase, f_1^{ini}, fraction of oxidation-prone phase which has not oxidized, f_2, fraction of oxidation products consisting of the primary oxide, f_{ox}, as well as a fraction of new metallic phase of volume fraction, f_3. All these four volume fractions make up the whole volume within the internal oxidation zone as defined below.

$$f_1^{ini} + f_2 + f_3 + f_{ox} = 1 \tag{6}$$

The constituents of the IOZ remain as the unsteady four phases as defined above until the primary oxidation is done. After the completion, two solid phase matrix of volume fractions which are oxidation resistant phase, f_1^{ini} and final product of newly formed metallic phase of volume fraction, f_3^f coexist within the IOZ in a steady state population either in large oxide or finely dispersed aggregates.

$$f_1^{ini} + f_3^f = 1 \tag{7}$$

By introducing a new internal state variable, *f*, which corresponds to a normalized fraction of the oxidizing phase, each variable in Eq. 6 can be expressed as below.

$$f_2 = (1 - f) f_2^{ini}, \tag{8}$$

$$f_3 = f f_3^f, \tag{9}$$

$$f_{ox} = f f_{ox}^f, \tag{10}$$

where *f* can vary in value from 0 to 1, which is from the time before the oxidation begins to the primary oxidation ends respectively. The final state of the primary oxide of volume fraction, f_{ox}^f is defined as in Eq. 11,

$$f_{ox}^f = r_{ox} \frac{(f_2^{ini} + \Delta f_{ox})}{(1 + \Delta f_{ox})} \tag{11}$$

where r_{ox} is the final volume fraction in the oxidized Phase 2, and Δf_{ox} is defined as,

$$\Delta f_{ox} = ln\{1 + f_2^{ini}[\exp(3e_V^T) - 1]\}. \tag{12}$$

In the Eq. 11, e_V^T is the mean local dilatational strain induced by the transformation of Phase 2, f_2. Lastly, the final volume fraction metallic phase, f_3^f can be defined as,

$$f_3^f = 1 - f_1^{ini} - f_{ox}^f. \tag{13}$$

The information of volume fractions throughout the oxidation process is really useful in understanding the mechanical behavior of the material constituents within the TGO layer and describing the stress-strain properties of the materials.

3.3.2 FORMULATION OF STRESS-DIFFUSION EQUATION

The aggregated stress, **T** that builds up within the TGO layer can be modeled using hypoeleastic formula which can be expressed in terms of the Jaumann derivate of stress **T,** as shown below,

$$\overset{\nabla}{\mathbf{T}} = \mathcal{L}[\mathbf{D} - \mathbf{D^{in}}] - 3\kappa\alpha\dot{\theta}\mathbf{1} \tag{14}$$

where **D** is the stretching tensor,$\mathbf{D^{in}}$ the inelastic strecthing tensor associate with the deformation, $\dot{\theta}$, the rate of change of absolute temperature, α the thermal expansion coefficient. This formulation takes into account the effect of diffusion of oxidant species through the metal, the oxidation of its oxidation-prone phase and the effect of the local volumetric expansion of oxide it inelastic strain as well residual stress. In general, the Jaumann deribvative of the stress is expressed as in Eq. 15.

$$\overset{\nabla}{\mathbf{T}} = \dot{\mathbf{T}} - \mathbf{WT} + \mathbf{TW} \tag{15}$$

where **W** is the total material spin. The inelastic stretching tensor in Eq. 14 is associated with the average inelastic stretching tensor rate due to creep, $\mathbf{D^{cr}}$**,** and a non-recoverable deformation rate due to the oxidation of one of the metallic phase, $\mathbf{D^{tr}}$, as shown below.

$$\mathbf{D^{in}} = \mathbf{D^{cr}} - \mathbf{D^{tr}} \tag{16}$$

where D^{cr} represents the volume fraction weighted sum of the individual components of each phase, $\dot{\mathbf{e}}_{\boldsymbol{i}}^{\boldsymbol{cr}}$ as presented below,

$$\mathbf{D^{cr}} = \sum_{\mathbf{i}} f_i \dot{\mathbf{e}}_{\boldsymbol{i}}^{\boldsymbol{cr}} \tag{17}$$

and D^{tr} is controlled by the rate of change of the internal oxidation $\dot{f}$,

$$\mathbf{D^{tr}} = f_2^{ini} \dot{f} \left\{ \sqrt{\frac{3}{2}} P \frac{\mathbf{T'}}{\check{\mathbf{S}}} + e_V^T \mathbf{1} \right\} \tag{18}$$

$$\dot{f} = (1-f)\dot{N}_p V_p \text{ for } C_O \geq C_{Ocr} \qquad \text{else } \dot{f} = 0, \tag{19}$$

where in Eq. 18, P is a shape coefficient of the oxide particles, $\check{S}$ the norm component of the stress tensor and **T'** is the deviatoric component of **T.** Whereas in Eq. 19, which is based on nucleation kinetics, $\dot{N}_p$ and $\dot{V}_p$ are the rate of increase of oxide precipitates per unit volume and the average volume of each oxide particle, respectively. The local oxygen concentration is denoted as C_O and the temperature-dependent critical concentration is assigned with C_{Ocr}, which is calibrated from oxidation data. Then, a stress tensor rate that accounts each oxidizing and non-oxidizing phase, $\dot{\sigma}$ is introduced as,

$$\dot{\sigma}_i = \dot{\mathbf{T}} + 2\mu(1-\beta)\left\{\mathbf{D^{cr}} - \dot{\mathbf{e}}_{\boldsymbol{i}}^{\boldsymbol{cr}} - \dot{\mathbf{A}}_{\mathbf{i}}\right\} \tag{20}$$

where μ is the viscosity, β the Eshleby's elastic accommodation factor and $\mathbf{A_i}$ is introduced as an additional interphase accommodation tensorial variables in order to describe the interaction between coexisting phases such as elastic oxide and creeping metallic phases. The rate of change of $\mathbf{A_i}$ is then defined as,

$$\dot{\mathbf{A}}_{\mathbf{i}} = \widehat{H}(f,\theta)\left\{\sum_k f_k \mathbf{S}_k \left|\dot{e}_k^{cr}\right| - \mathbf{S}_i \left|\dot{e}_i^{cr}\right|\right\} \tag{21}$$

where $\widehat{H}(f,\theta)$ is a dimensionless homogenization function that is calibrated from experimental data and Finite Element calculation, which is provided in Busso's paper (Journal de Physique). In

Eq. 21, $\mathbf{S_i}$ is another phase accommodation variable tensor for each phase that is defined as below.

$$\dot{\mathbf{S}}_\mathbf{i} = \dot{\mathbf{e}}_{\boldsymbol{i}}^{\boldsymbol{cr}} - \widehat{H}(f,\theta)\mathbf{S}_i\left|\dot{\bar{e}}_i^{cr}\right| \tag{22}$$

The stress of oxidizing and non-oxidizing phase, σ_i formula is later written in Fortran code in order to be applied numerically in ANSYS.

This formulation work, however, does not account the effects of interdiffusion processes that are driven by concentration gradient between the metallic coating and the substrate on the composition of the oxidized material and on the coating microstructure for the sake of simplification. The interdiffusion process is identified to have the ability to raise the oxide volume fraction up to 100% of the oxidized material and this may result in local stress increment. Nonetheless, the effects of interdiffusion processes are still neglected since the interdiffusion time is considered longer than primary oxidation time, the time taken to diminish all the NiAl phase of Al in a NiCoCrAly bond coat layer [12]. Thus, it is reasonable to assume that those effects may be less significant than the primary oxidation as discussed in Busso's paper [3].

3.4 FRACTURE MECHANICS APPROACH

There are several papers [8, 9, 21, 22] that introduce fracture mechanics as a practical method to determine the damage criteria of TBC layers. This approach uses the calculation of the stress and stress intensity factor, *K*, on a local crack area, where focus is placed only on a small local part instead of the entire component. The steps consist of determining a certain model shape on the local area that already has a pre-existing crack as shown in Fig. 3(a). The crack that exists within

the TBC layer is important in calculating the stress intensity factor, *K*, for a given loading value. The value of *K* can also be later used in determining energy release rate, *G*. To decide failure, the value of *K* of the material is compared with the model's fracture toughness property, K_{IC}.

Another method of modeling is to locally define a circle-shaped model around the peak of undulation as shown in Fig. 3(b). By doing so, stress calculation within the TGO layer can be simplified and defined as hoop stress. Hence, using the simplified stress definition, the maximum normal and acting stress can be calculated and compared to the yield strength of the TGO layer.

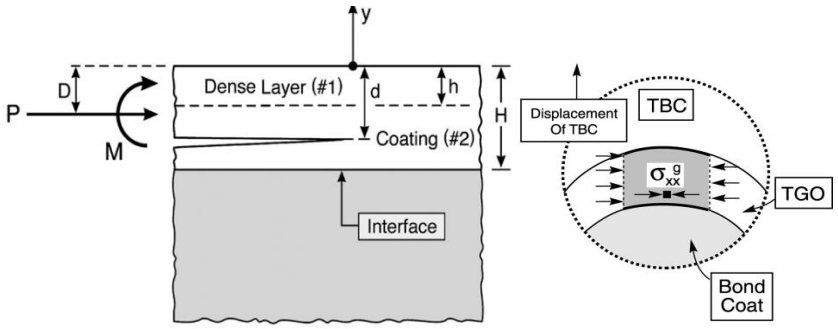

Figure 3: a) Model of a local TBC layer with a pre-existing crack. b) A circle-shaped model of a local TBC layer at the peak of undulation (imperfection) [8,9].

This method is relatively reliable with the condition that a crack location is known or the undulation behavior (amplitude and wavelength) is given from experiment. Unfortunately, this approach has its own limitation, as it does not fulfill this project's main purpose. As indicated earlier, this paper intends to predict the lifetime of the TBC layer from the beginning of the turbine's operation without having any pre-existing crack or undulations. In addition, the crack models of the TBC always vary between reviewed papers. Thus, due to all these restrictions, this method will not be applied in our computer simulation.

4.0 CHALLENGES

One of the main challenges in this project is to find the material properties of each TBC layer (TC, TGO and BC) such as its thermal conductivity and elastic modulus. The process presents a challenge because the information obtained from previous experiments and studies are insufficient. This is because some of the experimental data does not provide important material properties that are temperature dependent. On top of that, material properties of the specimen obtained from experiment may differ as it depends on the grain size and roughness of the TBC surface as well. A comprehensive finding is required in order to adequately gather information of the layers.

Another challenge is to ensure the method that will be chosen from the selection above can be easily implemented in finite element (FE) computation. In conducting the finite element analysis, we have to consider what type of assumptions and limitations that has to be made in order to get a reasonable result that can be compared to any hands on experiment. We would also like to ensure the FEA modeling suggested can be incorporated into a much more complicated thermal application such as commercial turbine blade in an extreme temperature condition. If the method chosen is too complex, it will be very complicated to implement in finite element computation and we may end up with inaccurate results. For example, a coupled oxidation constitutive approach as discussed earlier is considered difficult to carry out as it involves three types of analysis - diffusion or oxidation process, thermal analysis and structural analysis. This is

not possible via a basic ANSYS application because the software is limited to a coupled analysis such as thermal-structural analysis only. An additional process would require complicated programming and customization.

The last challenge is to make sure that the method selected may serve our research group's purpose in predicting the lifetime of the TBC of a turbine blade application from the start of its operation. In the beginning of a TBC's life, fractures do not yet form as they normally occur after a few hundred hours of thermal operation. Hence, we would like to choose a method that will not depend on fracture or crack behavior. The fracture mechanics method is not a viable option because we intend to use an all encompassing method that can provide a quick and practical solution to model TBC layers regardless of its operating conditions and the complexity of its 3-D geometry.

5.0 FINITE ELEMENT IMPLEMENTATION

5.1 MODELING PROCEDURE

In finite element modeling, we model a three-dimensional square supper alloy coupon with its top surface shielded by a layer of TBC. The solid model is meshed with a conventional SOLID70 element while the SHELL132 element that is used for TBC layer consists of top coat, BC and TGO. SHELL132 is selected due to its reliability in thin layer application. In addition, it provides an option for users to directly mesh SHELL elements with SOLID elements that have significantly different thickness and volume as shown in Figure 4. Application of SHELL132 elements may increase computational speed while maintaining the simulation stability of the multi-layered insulation. As can be seen in Figure 4, we assign SHELL132 element with three layers that correspond to top coat, TGO and bond coat layers. In addition, SHELL132 element allows user to improve the accuracy of simulation results by simply stacking more layers within the element.

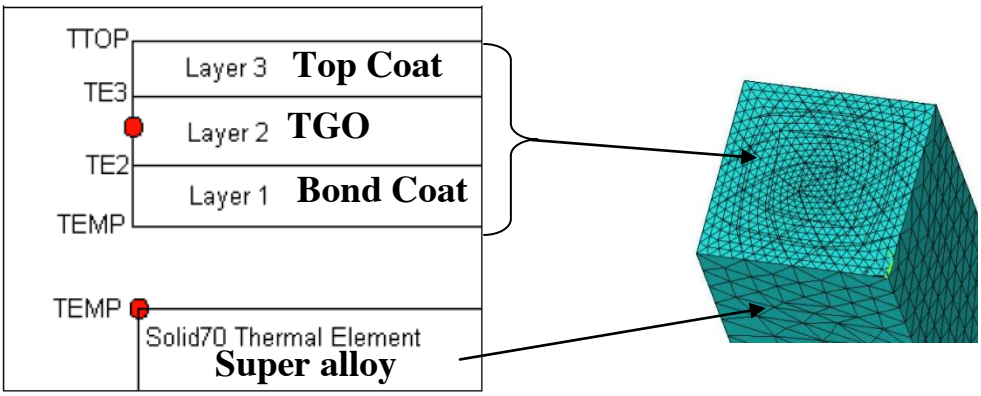

Figure 4: SHELL element for thin layers can be directly meshed directly to SOLID thermal elements with thicker volume.

5.2 PRELIMINARY VERIFICATION OF SIMULATION

The first process is to check whether the computer simulation of TBC layers can produce a credible result. Verification is done by comparing our simulation result with experimental data obtained by Limarga [10]. In his study, as shown in Figure 5, a small coupon of TBC is gradually heated up until it reaches 1200 ˚C for 60 seconds. Then the coupon is held for another 240 seconds, allowing the heat to distribute throughout the coupon. In the experiment, the stress distribution on the TBC layer is measured using Raman spectroscopy.

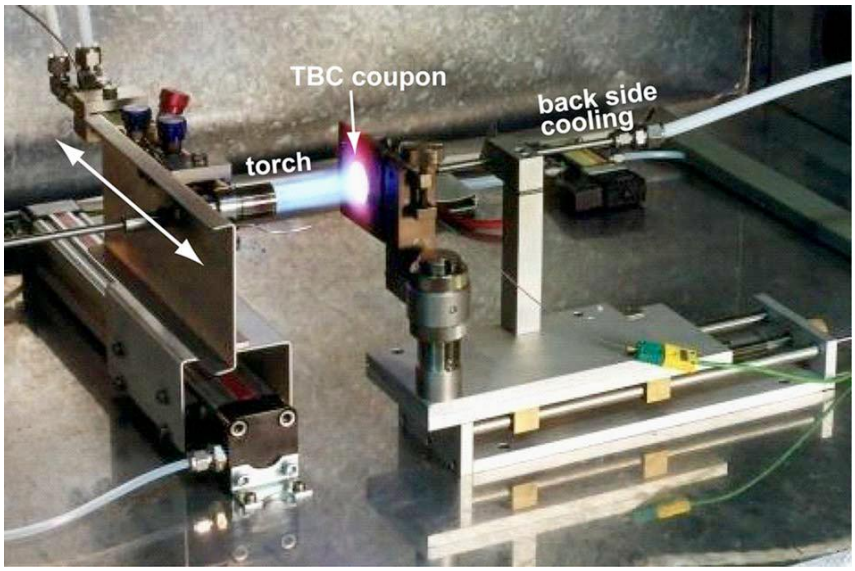

Figure 5: Experimental Setup for TBC coupon heating process [10].

In our finite element simulation, only one fourth of the coupon will be modeled as it allows us to apply sufficient thermal boundary conditions in the simulation such as zero heat flux at the lines of symmetry.

We apply heat at a temperature of 1200 ºC on the top layer of the model in thermal analysis and later observe the local stress on each layer during structural analysis. Below is the results obtained from the simulation. Figure 6 shows the distribution of stress on each layer within the TBC (TC, TC/TGO interface, BC/TGO interface) at time t = 60 seconds where the coupon reaches a temperature of 1200 ºC. Figure 7 shows the distribution of stress at time 300 seconds after the coupon is held to allow distribution of heat throughout the layers.

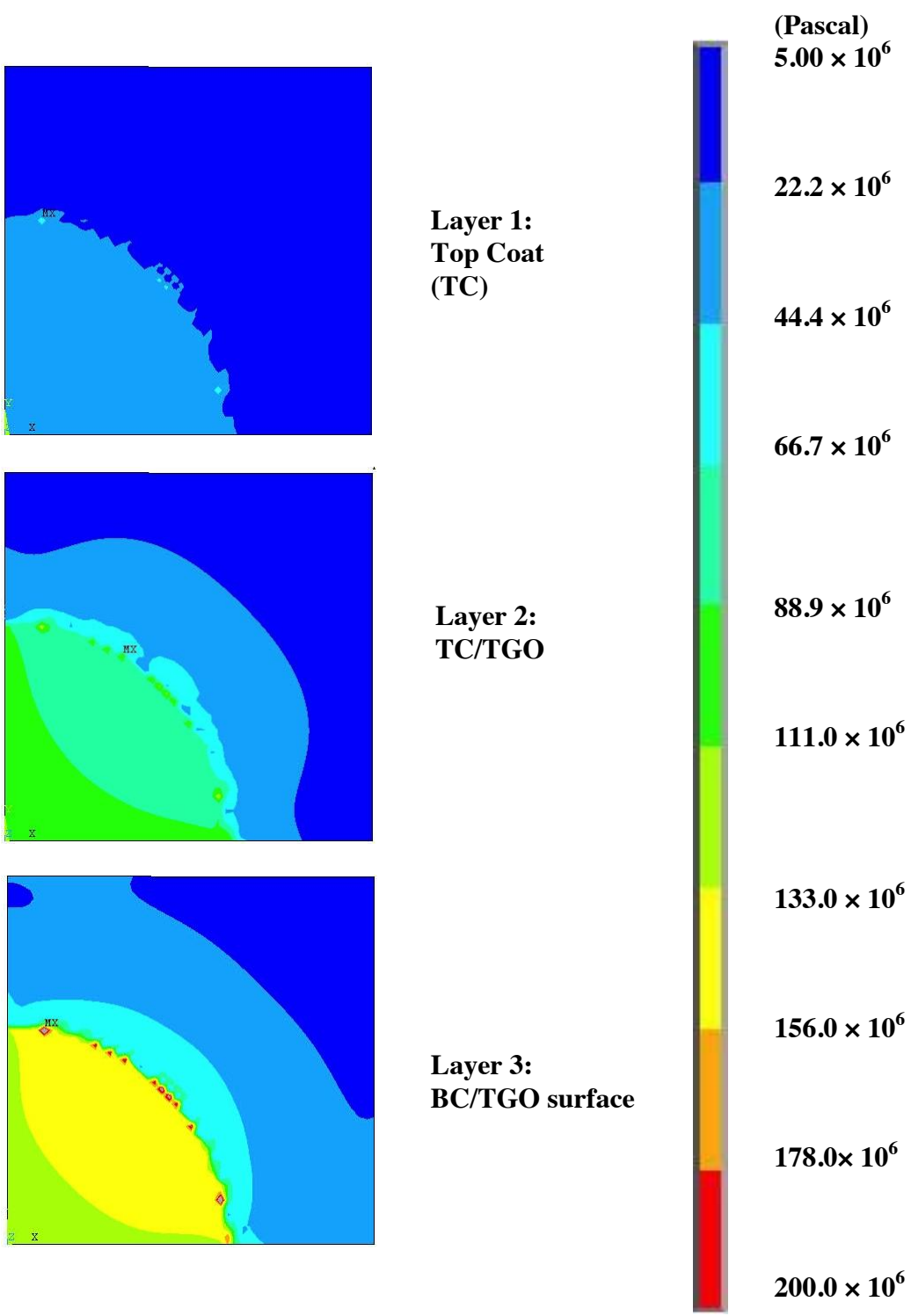

Figure 6: Stress (von Mises) distribution within TBC layers during heating process (t = 60 seconds).

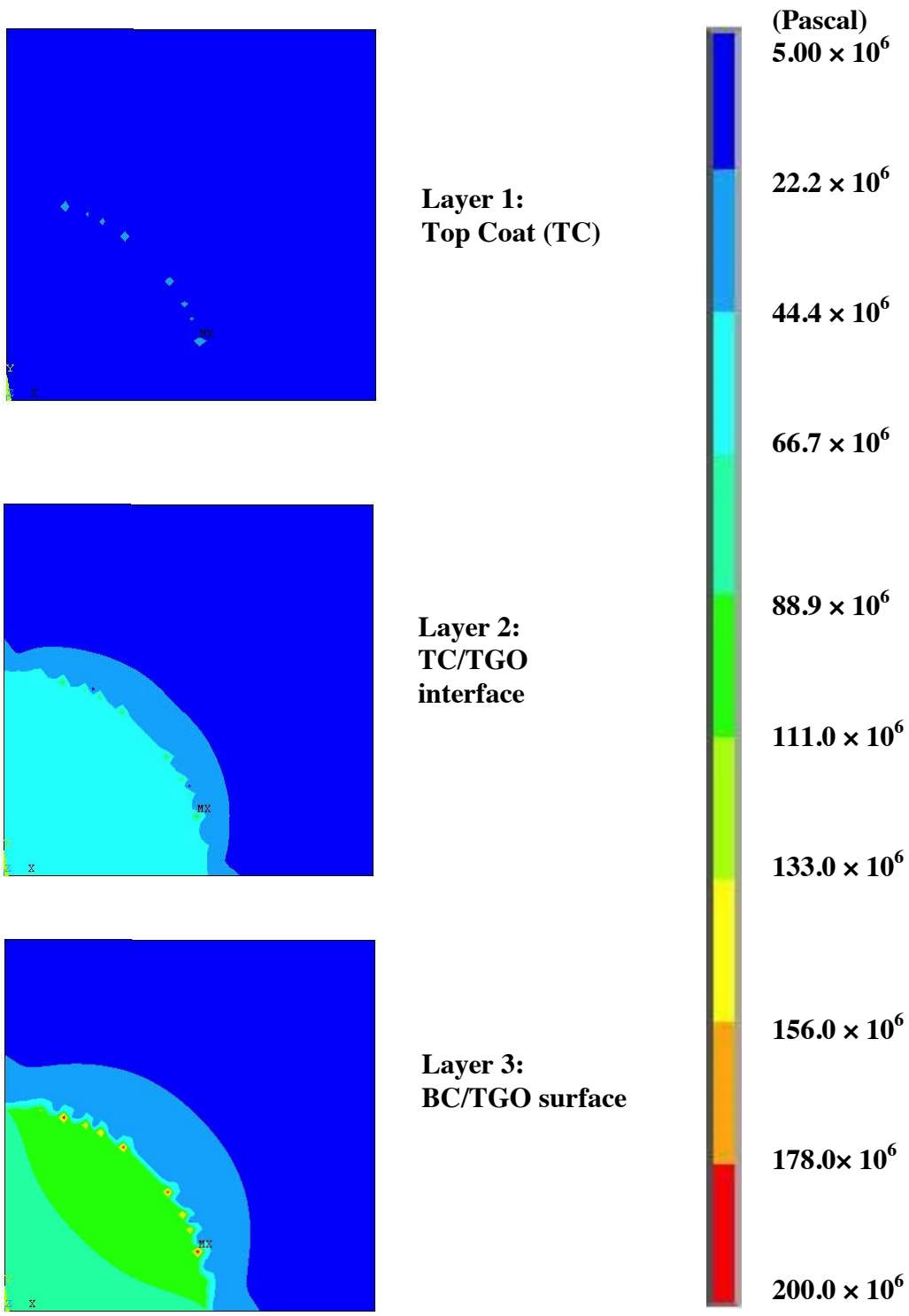

Figure 7: Stress (von Mises) distribution within TBC layers at the end of holding period (t = 300 seconds).

Result above shows that in general, the bond coat layer has a higher stress distribution compared to the top coat surface and TC/TGO interface. By comparing Fig. 6 and 7, it is interesting to note that the stress value is higher at the end of the heating process where the temperature difference between the top coat layer and bond coat layer is still high. As it reaches 240 seconds, temperature difference stabilizes at 400ºC while maximum von Mises stress value gradually drops.

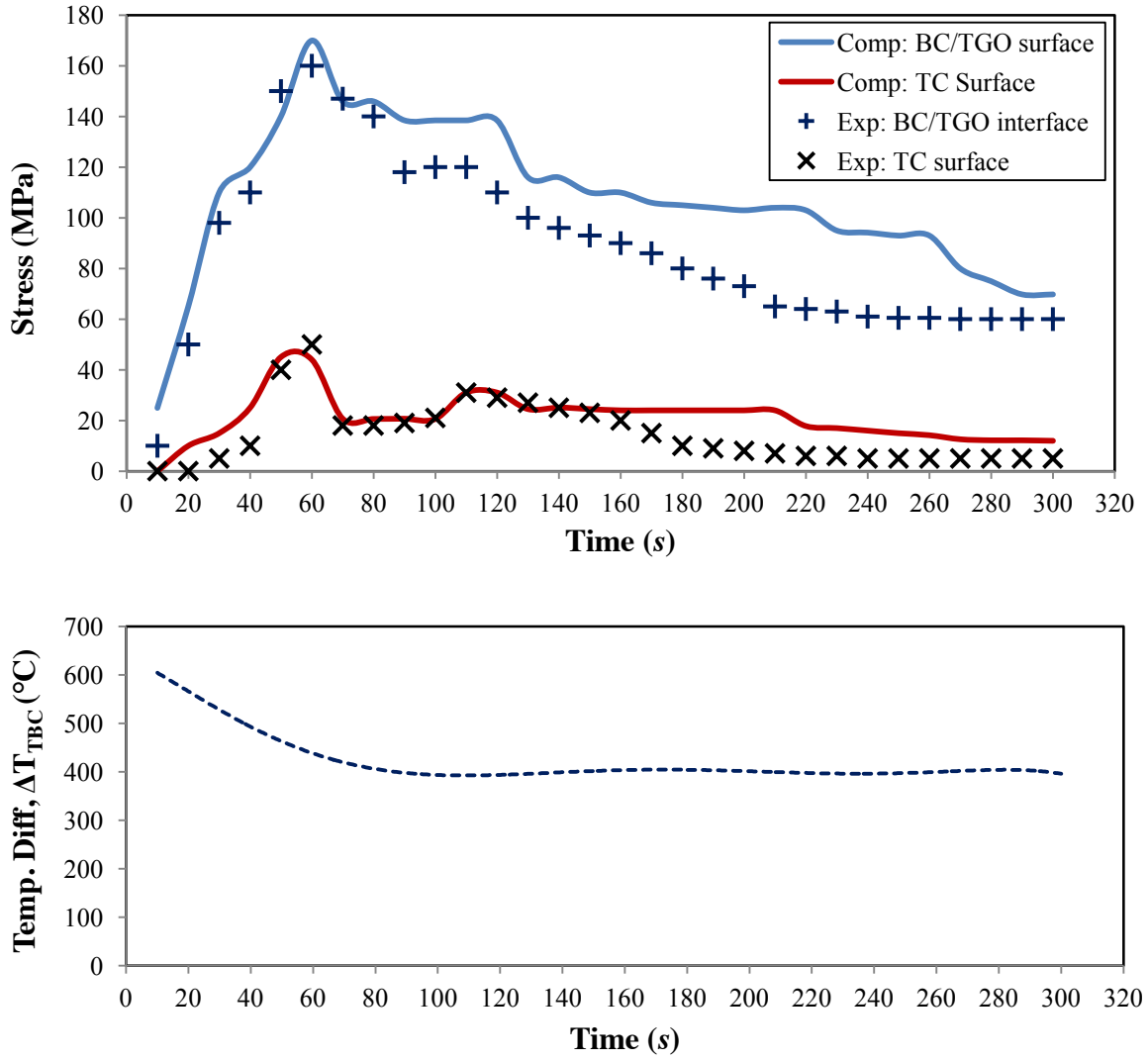

Figure 8: Evolution of stresses within the TBC layers and the temperature difference between TC surface and BC/TGO interface.

During the heating process, from time 0 to 60 seconds, the temperature difference, ΔT, between the top TC surface and lower BC surface is as high as 600ºC. During the holding period of 240 seconds the temperature drop slowly decreases as the BC layer picks up heat. Also, the temperature difference slowly drops and stabilizes at $\Delta T = 400$ºC. The Raman measurement from the experimental data indicates that the measured stresses in the coating are smaller than our predicted finite element analysis as shown in Figure 8. Nevertheless, the stress behavior does agree with experimental results where the stresses increase quite linearly during heating and slowly drop as the temperature difference, ΔT decreases during the holding process. The agreement obtained in this preliminary simulation gives us the confidence to further apply our finite element computation for both TGO thickness calculation as well as elasticity and creep effect analysis.

6.0 RESULTS

6.1 RESULT: TGO THICKNESS CALCULATION

Equations (1), (2) and (3) are used to calculate the final thickness of the TBC layer. TGO thickness vs. time plot was obtained in Figure 5 below.

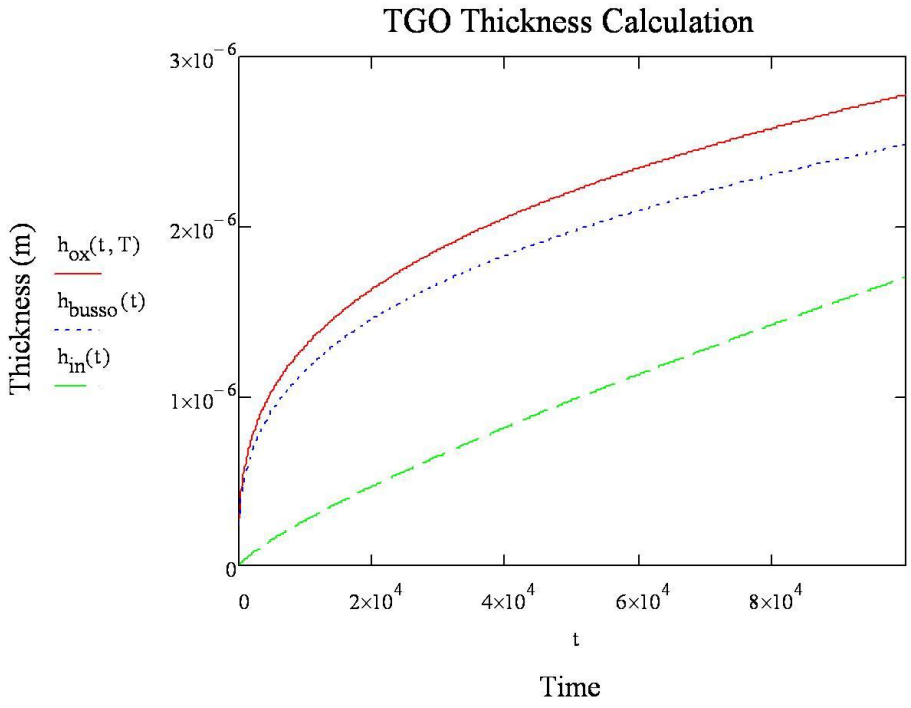

Figure 9: TGO thickness plot using Busso's and Echsler's models for operating temperature 1100ºC.

The graph shows that Echsler's thickness formulation expects higher thickness on the outside surface compared to Basso's thickness calculation. After 8000 hours of operation at temperature of 1100ºC, the thickness of the TGO is listed below,

Table 6: TGO thickness calculation based on Echsler's and Busso's formulations

Methods	***Thickness (µm)***
Echsler's Inward	1.3
Echsler's Outward	2.5
Busso	2.2

The thickness of TBC layer increases with increasing operation time and lifetime. In addition, all formulations predict a thickness value of TGO below the critical thickness values as mentioned earlier that is around 10 to 12 µm. Since the simulation only runs for a period of 8000 hours, we can observe that the thickness obtained is also below Karaivanov's simulation [11] of TBC thickness, which is around 12.6 µm for 1600 hours operation.

The equations (1), (2) and (3) can be implemented in Ansys post-processing. This process can be applied on any 3-D geometry of thermal applications. The model used is a turbine blade model overlaid with SHELL132. Below is the result of the simulation on a turbine blade that is operating at a temperature of 1100ºC for 1000 hours only. The simulation result expects lower TGO thickness since the operating period is short.

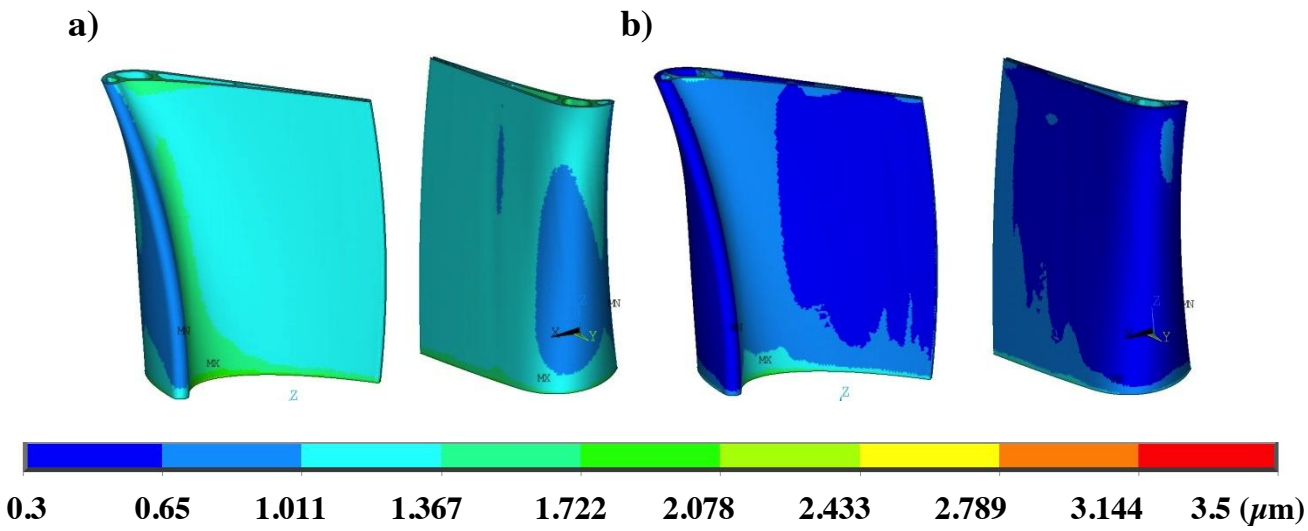

Figure 10: TGO thickness contour plots on a turbine blade at temperature of 1100ºC for 1000 hours. a)Echsler's model. b)Busso's model.

Most of the reviewed papers recognize that the thickness of the TGO layer seems to be one of the most important factors in determining a TBC's lifetime. The method appears simple and plausible. Unfortunately, it lacks any clear and defining failure criteria. Hence, to depend only on the TGO thickness calculation for TBC lifetime prediction may be insufficient.

6.2 RESULT: LOCAL STRESS DISTRIBUTION

To implement the creep effect and elasticity method, we assume the thickness of the TGO to be constant at 3 μm, while the thicknesses for bond coat and top coat (YSZ) layers are set to 150 μm and 500 μm respectively. The simulation is run at a steady state for 700 hours at operating temperatures of 800ºC and 1100ºC and 1300ºC. Figure 11 below shows the local stress distribution on each layer.

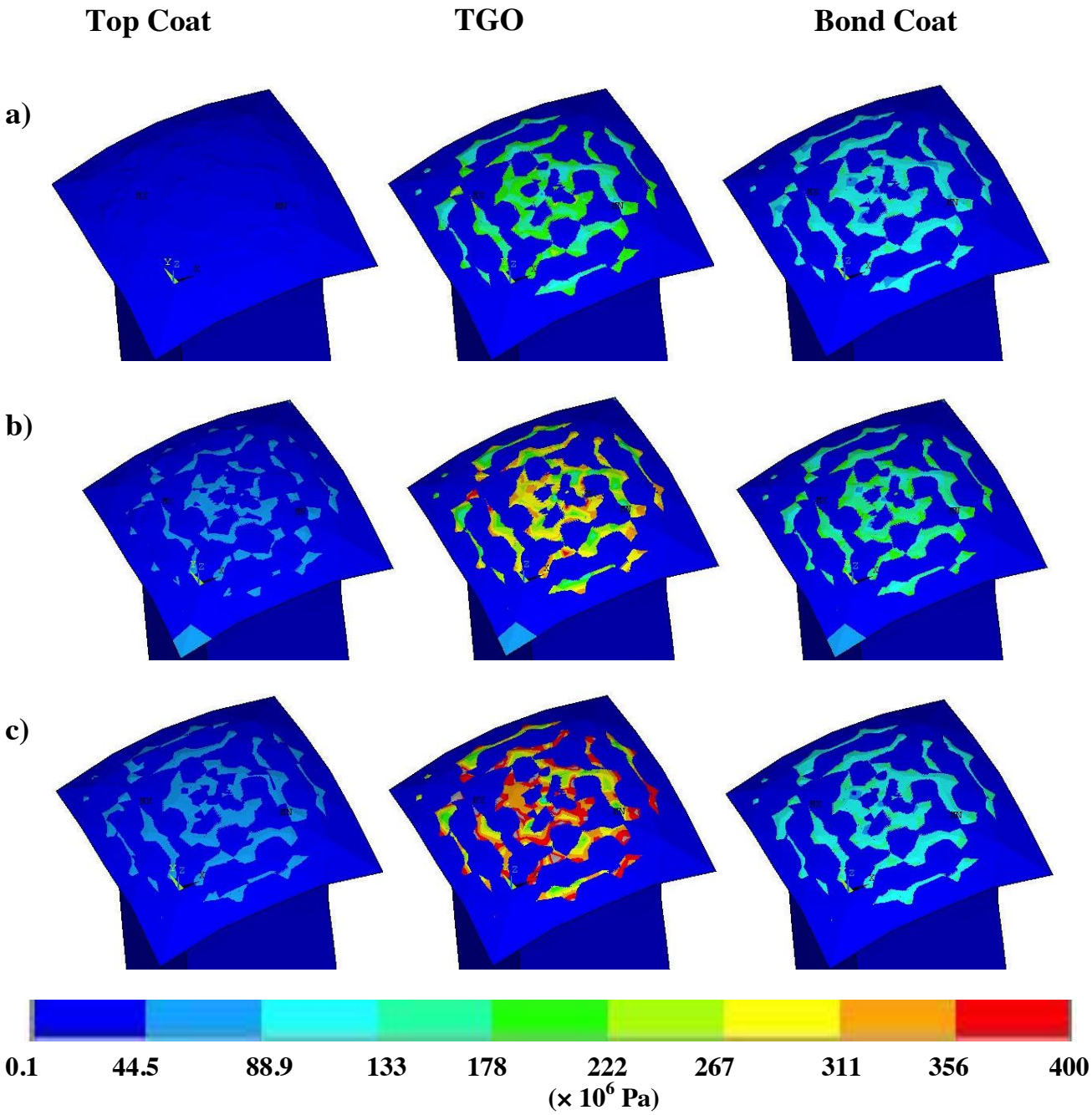

Figure 11: Local von Mises stress distribution on TC, TGO and BC layers at temperature of a)800ºC b)1100ºC c)1300ºC after 730 hours.

To better understand the stress distribution for each layer, we plot the maximum local von Mises stress for each layer and compare it at different operating temperatures (880ºC, 1100ºC and 1300ºC).

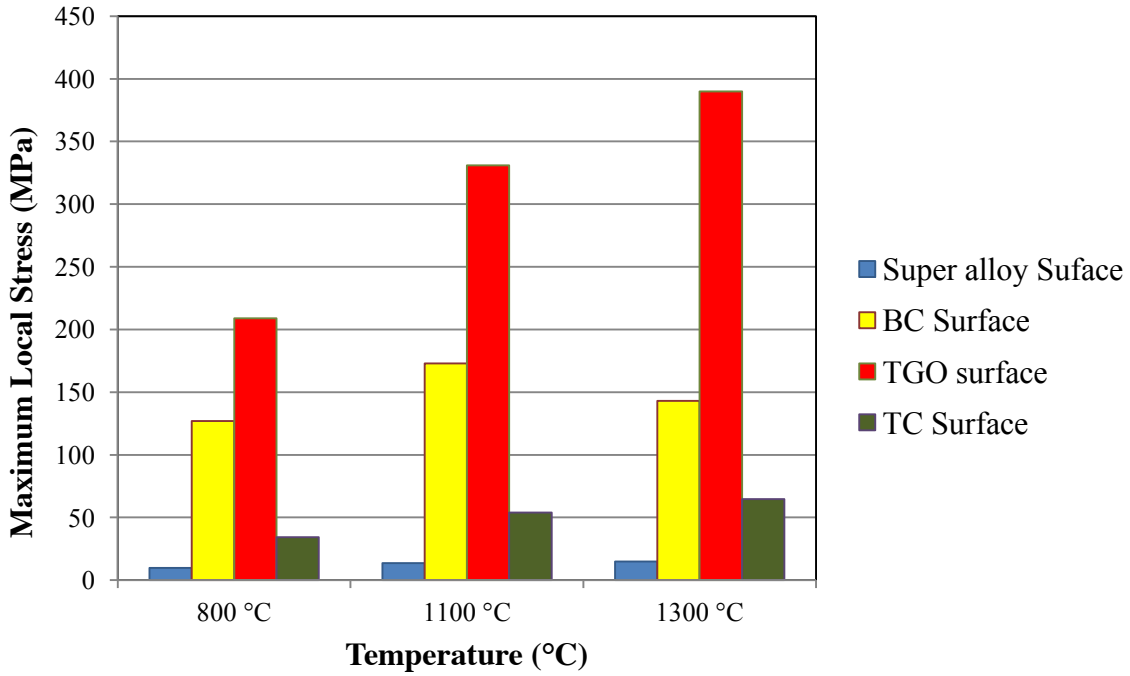

Figure 12: Maximum local von Mises stress for each TBC layer including super alloy surface.

The result shows that the stress is higher on TGO layer in comparison to other layers regardless of operating temperatures. As the operating temperature increases, the local stress also increases. The maximum local stresses in the result are still lower than maximum local stress reported in Hsueh et. al work [27]. The result also shows that the stresses in the TBC layer are in the range of 5 MPa to 400 MPa, which is a reasonable value as we discussed earlier in the preliminary verification process. The super alloy has the lowest local stress value, which might be because the TBC layer protects it thermally. Overall, this result is very useful as it can be used in comparing with future experimental data.

6.3 FAILURE CRITERIA

In this study the failure criteria used is simply based on maximum yield stress due to the limitation of our FEA, which is only in elastic region. We create a condition which can signal for impending failure when the any of the TBC layers such as TGO, BC, TC has local von Mises stress that is multiple times higher than its yield strength, depending on the safety factor assigned on a design. Hence, this criteria is incorporated in ANSYS by setting manually the formula below

$$D = \frac{\sigma_{local}}{FOS \times \sigma_Y} \tag{23}$$

where value D is the damage parameter, FOS is the safety factor with a typical value of 3 to 6.5 for general NASA turbine blade or any thermal application and σ_Y is the yield strength.

Based on equation (23), if D is larger than 1, it means one of the TBC layers has yield and may possibly experience an impending failure. This failure theory however may be replaced with other suitable failure indicators depending on various needs. Figure 13 below shows the damage D parameter contour plot for TBC layer operating at 800ºC for 730 hours.

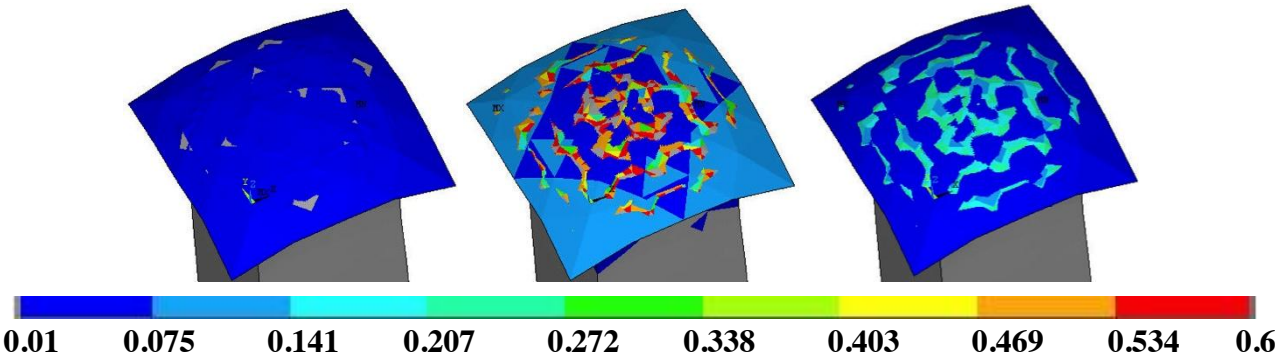

Figure 13: Contour plot of damage parameter D on each layer of TBC at 800ºC and 730 hours.

7.0 SUMMARY AND CONCLUSION

There are four available methods to predict lifetime of TBC layers as discussed in this work. Of all the methods, TGO thickness calculation and creep effect and elasticity analysis are used in finite element analysis because both methods are applicable to finite element computation and can serve the purpose of our project.

TGO thickness calculation method applied in finite element computation is improved upon from the previous work done by Karaivanov [11] as the calculation of the thickness is now based on the particular layer of TBC instead of just the alloy layer. The result obtained is promising but it does not have detailed information on the behavior of each TBC layer such as stress distribution. In addition, the method still currently does not have one specific critical thickness value when the TBC happens to fail as current research work provides different views on critical thickness value.

The simulation results of the creep and elasticity analysis are, generally, in agreement with experimental data obtained from Limarga's work [10] as the stress values of the layers are considered within a reasonable range. The simulation result, however, may have overestimated the value of stresses on each of TBC layers as it does not consider grain roughness of each surface and various significant effects that occur within the TBC layer such as sintering and cracking effects. The effect of cracking may result in changes to the elastic modulus of the TBC

layer. As a result, the random location of cracks within the layer may create nonuniform stress distribution.

In addition the presence of crack may release some stresses, lowering the local stress values within the layers. On the other hand, sintering, which usually occurs at a higher rate, may increase thermal conductivity and elastic modulus of the TBC layer. The presence of both sintering and cracking may create complex elastic modulus and stress behavior within the coating. Besides, the constitutive behavior of sintering is less known while the cracking behavior is highly dependent on rough grain as well as temperature, making the study more complex and beyond the scope of our study. Thus, it is very important to understand the slight discrepancy of the simulation result due to the limitations mentioned above before applying it into finite element computation.

To overcome this shortage, more advanced yet complex methods like A Coupled Oxidation Constitutive Approach may need to be used in order to improve stress prediction of TBC layers. Nevertheless, the research has shown that the TBC layers can be easily modeled in finite element computation and may still be useful with other thermal application such as turbine blades.

Moreover, it is important to consider that in this simulation, we have assumed that all the layers (top coat, bond coat, TGO) have isotropic material properties. The assumption is made due to limited experimental data of the layers. The calculation of local stresses can be significantly affected from the assumption. Hence, to improve our results, more defined material properties of TBC are required.

To obtain accurate results, one of the important computational aspects that needs to be considered is mesh refinement. As shown in Fig. 11 and 13, the stress distribution on the TBC

surface is not entirely uniform as there is a significant variation in stress value between bright spots and their surroundings. These bright spots have higher stress values from the surroundings. The spots are essentially the SHELL132 (TBC) elements that are perfectly attached with the SOLID70 (super alloy) elements underneath. These bright spots give more reasonable stress values. On the other hand, the darker surrounding areas are the SHELL132 (TBC) elements that are not completely attached to SOLID70 (super alloy) elements. As a result, the stress values of these darker areas are relatively low and may not be quite precise. To overcome this problem, one method includes refining the mesh. Mesh refinement will create more SHELL132 elements, allowing higher number of SHELL132 elements to be attached with SOLID70 elements. However, due to the constraint of our computer's processing capability, only a restricted number of SHELL32 elements can be generated, resulting in less amount of SHELL132 elements that can be connected with SOLID70 elements.

For future studies, data from this experimental analysis can be of benefit so that more experimental data for this specific case can be obtained and be used to verify the validity of the simulation result. Overall, the finite element computation seems successful to the point where it manages to predict stress behavior that occurs within each TBC layer.

APPENDIX A

SAMPLE ANSYS INPUT FOR POST-PROCESSING

```
! Echsler Outward Oxidation
!-------------------------------------------------------------
/POST1
SUSEL,S,
!Create Local CS at WP Origin
CSWPLA,9999
SUSEL,ALL,
SUSEL,ALL,
ETABLE,temp,TEMP,
!*
ETABLE,,ERASE,1
ETABLE,T1,TEMP,
!*
PLETAB,T1,AVG
PLETAB,T1,NOAV
SEXP,EXP1,T1, ,-1,1,
SMULT,MUL1,EXP1, ,-8385.14,1,
SEXP,MUL2,MUL1, ,2,1,
SEXP,MUL3,MUL1, ,3,1,
SEXP,MUL4,MUL1, ,4,1,
SADD,ADD1,MUL1,MUL2,1,0.166667,1,
ETABLE,,ERASE,7
SADD,ADD1,MUL1,MUL2,1,0.5,1,
SADD,ADD2,MUL3,MUL4,0.166667,0.041667,0,
SADD,ADDTotal,ADD1,ADD2,1,1,0,
SMULT,TGO,ADDTOTAL, ,0.005843,1,
PLETAB,TGO,NOAV
!-------------------------------------------------
```

```
!Busso Calulation


SADD,STEP2ADD,EXP1, ,1,1,-0.000413,
SMULT,STEP3MUL,STEP2ADD, ,-9224.88,1,
SEXP,STEP3MUL2,STEP3MUL, ,2,1,
SEXP,STEP3MUL3,STEP3MUL, ,3,1,
SEXP,STEP3MUL4,STEP3MUL, ,4,1,
/DIST,1,1.08222638492,1
/REP,FAST
/DIST,1,0.924021086472,1
/REP,FAST
ETABLE,REFL
ETABLE, ,TF,X
!*
ETABLE,,ERASE,13
SEXP,STEP3MUL2,STEP3MUL, ,2,1,
SEXP,KUASA2,STEP3MUL, ,2,1,
SEXP,KUASA3,STEP3MUL, ,3,1,
SEXP,KUASA4,STEP3MUL, ,4,1,
SADD,STEP4ADD1,STEP3MUL,KUASA2,1,0.5,0,
ETABLE,,ERASE,16
ETABLE,,ERASE,12
ETABLE,,ERASE,15
ETABLE,,ERASE,14
ETABLE,,ERASE,13
```

```
SMULT,KUASA1,STEP2ADD, ,-9224.88,1,
SEXP,KUASA2,KUASA1, ,2,1,
SEXP,KUASA3,KUASA1, ,3,1,
SEXP,KUASA4,KUASA1, ,4,1,
SADD,TAMBAH1,KUASA1,KUASA2,1,0.5,0,
SADD,TAMBAH2,KUASA3,KUASA4,0.16667,0.041
667,0,
SADD,TOTAL,TAMBAH1,TAMBAH2,1,1,1,
SMULT,TGOBUSSO,TOTAL, ,0.000216,1,
PLETAB,TGOBUSSO,NOAV
!*
/CONT,1,9,AUTO
/REPLOT
!*
SMULT,TGOBMOD,TGOBUSSO, ,100,1,
PLETAB,TGOBMOD,NOAV
!*
```

APPENDIX B

SAMPLE ANSYS INPUT FOR SIMULATION

```
!------------------create block-------------------

/PREP7

BLOCK,0,100,0,1000,0,100,

!--------Super Alloy mat. properties ---------

/REP,FAST
mat,1
MPTEMP,,,,,,,,
MPTEMP,1,373
MPTEMP,2,473
MPTEMP,3,573
MPTEMP,4,673
MPTEMP,5,773
MPTEMP,6,873
MPTEMP,7,973
MPTEMP,8,1073
MPTEMP,9,1173
MPTEMP,10,1273
MPTEMP,11,1373
MPTEMP,12,1473
MPTEMP,13,1573
MPDATA,KXX,1,,9
MPDATA,KXX,1,,10
MPDATA,KXX,1,,12
MPDATA,KXX,1,,13
MPDATA,KXX,1,,16
MPDATA,KXX,1,,19
MPDATA,KXX,1,,22.5
MPDATA,KXX,1,,25
MPDATA,KXX,1,,27.5
MPDATA,KXX,1,,35
MPDATA,KXX,1,,50
MPDATA,KXX,1,,45
MPDATA,Kyy,1,,9
MPDATA,Kyy,1,,10
MPDATA,Kyy,1,,12
MPDATA,Kyy,1,,13
MPDATA,Kyy,1,,15
MPDATA,Kyy,1,,16
MPDATA,Kyy,1,,19
MPDATA,Kyy,1,,22.5
MPDATA,Kyy,1,,25
MPDATA,Kyy,1,,27.5
MPDATA,Kyy,1,,35
MPDATA,Kyy,1,,50
MPDATA,Kyy,1,,45
MPDATA,Kzz,1,,9
MPDATA,Kzz,1,,10

MPDATA,Kzz,1,,12
MPDATA,Kzz,1,,13
MPDATA,Kzz,1,,15
MPDATA,Kzz,1,,16
MPDATA,Kzz,1,,19
MPDATA,Kzz,1,,22.5
```

```
MPDATA,Kzz,1,,25
MPDATA,Kzz,1,,27.5
MPDATA,Kzz,1,,35
MPDATA,Kzz,1,,50
MPDATA,Kzz,1,,45
MP,C,1,,630
MPTEMP,,,,,,,
MPTEMP,1,300
MPTEMP,2,473
MPTEMP,3,673
MPTEMP,4,873
MPTEMP,5,1073
MPTEMP,6,1273
MPTEMP,7,1373
MPDATA,EX,1,,125e+9
MPDATA,EY,1,,125e+9
MPDATA,EZ,1,,125e+9
MPDATA,PRXY,1,,.3875
MPDATA,PRYZ,1,,.3875
MPDATA,PRXZ,1,,.3875
MPDATA,GXY,1,,119e+9
MPDATA,GYZ,1,,119e+9
MPDATA,GXZ,1,,119e+9
MPDATA,EX,1,,118e+9
MPDATA,EY,1,,118e+9
MPDATA,EZ,1,,118e+9
MPDATA,PRXY,1,,.38
MPDATA,PRYZ,1,,.38
MPDATA,PRXZ,1,,.38
MPDATA,GXY,1,,112e+9
MPDATA,GYZ,1,,112e+9
MPDATA,GXZ,1,,112e+9
MPDATA,EX,1,,110e+9
MPDATA,EY,1,,110e+9
MPDATA,EZ,1,,110e+9
MPDATA,PRXY,1,,.379
MPDATA,PRYZ,1,,.379
MPDATA,PRXZ,1,,.379
MPDATA,GXY,1,,106e+9
MPDATA,GYZ,1,,106e+9
MPDATA,GXZ,1,,106e+9
MPDATA,EX,1,,104e+9
MPDATA,EY,1,,104e+9
MPDATA,EZ,1,,104e+9
MPDATA,EZ,1,,104e+9
MPDATA,PRXY,1,,.38
MPDATA,PRYZ,1,,.38
MPDATA,PRXZ,1,,.38
MPDATA,GXY,1,,98e+9
MPDATA,GYZ,1,,98e+9
MPDATA,GXZ,1,,98e+9
MPDATA,EX,1,,97e+9
MPDATA,EY,1,,97e+9
MPDATA,EZ,1,,97e+9
MPDATA,PRXY,1,,.381
MPDATA,PRYZ,1,,.381
MPDATA,PRXZ,1,,.381
MPDATA,GXY,1,,91.7e+9
MPDATA,GYZ,1,,91.7e+9
MPDATA,GXZ,1,,91.7e+9
MPDATA,EX,1,,90e+9
MPDATA,EY,1,,90e+9
MPDATA,EZ,1,,90e+9
MPDATA,PRXY,1,,.38
MPDATA,PRYZ,1,,.38
MPDATA,PRXZ,1,,.38
MPDATA,GXY,1,,85e+9
MPDATA,GYZ,1,,85e+9
MPDATA,GXZ,1,,85e+9
MPDATA,EX,1,,86e+9
MPDATA,EY,1,,86e+9
MPDATA,EZ,1,,86e+9
MPDATA,PRXY,1,,.38
MPDATA,PRYZ,1,,.38
MPDATA,PRXZ,1,,.38
MPDATA,GXY,1,,82e+9
MPDATA,GYZ,1,,82e+9
MPDATA,GXZ,1,,82e+9
!*
MPTEMP,,,,,,,
MPTEMP,1,300
MPTEMP,2,373
MPTEMP,3,473
MPTEMP,4,573
MPTEMP,5,673
MPTEMP,6,773
MPTEMP,7,873
MPTEMP,8,973
MPTEMP,9,1073
```

```
MPTEMP,10,1173
MPTEMP,11,1273
MPTEMP,12,1373
MPTEMP,13,1473
MPTEMP,14,1573
MPTEMP,15,1673
MPTEMP,16,1773
MPDATA,DENS,1,,8700
MPDATA,DENS,1,,8665
MPDATA,DENS,1,,8618
MPDATA,DENS,1,,8572
MPDATA,DENS,1,,8525
MPDATA,DENS,1,,8479
MPDATA,DENS,1,,8433
MPDATA,DENS,1,,8387
MPDATA,DENS,1,,8342
MPDATA,DENS,1,,8296
MPDATA,DENS,1,,8251
MPDATA,DENS,1,,8206
MPDATA,DENS,1,,8161
MPDATA,DENS,1,,8116
MPDATA,DENS,1,,7736
MPDATA,DENS,1,,7646
!*
MPTEMP,,,,,,,,
MPTEMP,1,300
MPTEMP,2,1573
UIMP,1,REFT,,,300
MPDATA,ALPX,1,,18.8e-6
MPDATA,ALPX,1,,18.8e-6
MPDATA,ALPy,1,,18.8e-6
MPDATA,ALPy,1,,18.8e-6
MPDATA,ALPz,1,,18.8e-6
MPDATA,ALPz,1,,18.8e-6


!*
ET,1,SOLID87
!*
```

```
!------ TBC material properties ----------

!IN-738 nickel based super alloy

/PREP7
!*
MPTEMP,,,,,,,
MPTEMP,1,273
MPTEMP,2,923.15
MPTEMP,3,1073.15
MPTEMP,4,1173.15
MPTEMP,5,1273.15
MPDATA,KXX,1,,8.72
MPDATA,KXX,1,,19.66
MPDATA,KXX,1,,22.28
MPDATA,KXX,1,,24.03
MPDATA,KXX,1,,25.78
MPTEMP,,,,,,,,
MPTEMP,1,273
MPTEMP,2,923.15
MPTEMP,3,1073.15
MPTEMP,4,1173.15
MPTEMP,5,1273.15
MPDATA,C,1,,428
MPDATA,C,1,,594
MPDATA,C,1,,636
MPDATA,C,1,,675
MPDATA,C,1,,727
MPTEMP,,,,,,,,
MPTEMP,1,0
MPDATA,DENS,1,,8500
MPTEMP,,,,,,,,
MPTEMP,1,273
MPTEMP,2,923.15
MPTEMP,3,1073.15
MPTEMP,4,1173.15
MPTEMP,5,1273.15
UIMP,1,REFT,,,273
MPDATA,CTEX,1,,11.44
MPDATA,CTEX,1,,14.44
MPDATA,CTEX,1,,15.16
MPDATA,CTEX,1,,15.64
MPDATA,CTEX,1,,16.12
```

```
MPTEMP,,,,,,,
MPTEMP,1,0
MPDE,DENS,1
MPDATA,DENS,1,,8500
MPTEMP,,,,,,,
MPTEMP,1,273
MPTEMP,2,923.15
MPTEMP,3,1073.15
MPTEMP,4,1173.15
MPTEMP,5,1273.15
MPDATA,EX,1,,202E9
MPDATA,EX,1,,165E9
MPDATA,EX,1,,156E9
MPDATA,EX,1,,150E9
MPDATA,EX,1,,144E9
MPDATA,PRXY,1,,0.3
MPDATA,PRXY,1,,0.3
MPDATA,PRXY,1,,0.3
MPDATA,PRXY,1,,0.3
MPDATA,PRXY,1,,0.3
MPTEMP,,,,,,,
MPTEMP,1,273
MPTEMP,2,923.15
MPTEMP,3,1073.2
MPTEMP,4,1173.2
MPTEMP,5,1273.2
MPDE,EX,1
MPDE,PRXY,1
MPDATA,EX,1,,2.02E+011
MPDATA,EX,1,,1.65E+011
MPDATA,EX,1,,1.56E+011
MPDATA,EX,1,,1.5E+011
MPDATA,EX,1,,1.44E+011
MPDATA,PRXY,1,,0.3
MPDATA,PRXY,1,,0.3
MPDATA,PRXY,1,,0.3
MPDATA,PRXY,1,,0.3
MPDATA,PRXY,1,,0.3
```

```
!NiCrAlY bond coat
!-----------------
!*
MPTEMP,,,,,,,
MPTEMP,1,273
MPTEMP,2,773.15
MPTEMP,3,873.15
MPTEMP,4,973.15
MPTEMP,5,1073.15
MPTEMP,6,1173.15
MPTEMP,7,1273.015
MPTEMP,8,1373.15
MPDATA,EX,2,,152E9
MPDATA,EX,2,,136E9
MPDATA,EX,2,,133E9
MPDATA,EX,2,,128E9
MPDATA,EX,2,,117E9
MPDATA,EX,2,,100E9
MPDATA,EX,2,,74E9
MPDATA,EX,2,,41E9
MPDATA,PRXY,2,,0.3
MPDATA,PRXY,2,,0.3
MPDATA,PRXY,2,,0.3
MPDATA,PRXY,2,,0.3
MPDATA,PRXY,2,,0.3
MPDATA,PRXY,2,,0.3
MPDATA,PRXY,2,,0.3
MPDATA,PRXY,2,,0.3
MPTEMP,,,,,,,
MPTEMP,1,0
MPDATA,DENS,2,,7320
MPTEMP,,,,,,,
MPTEMP,1,273
MPTEMP,2,773.15
MPTEMP,3,873.15
MPTEMP,4,973.15
MPTEMP,5,1073.15
MPTEMP,6,1173.15
MPTEMP,7,1273.15
MPTEMP,8,1373.15
UIMP,2,REFT,,,273
MPDATA,CTEX,2,,12.59
MPDATA,CTEX,2,,14.33
MPDATA,CTEX,2,,14.97
MPDATA,CTEX,2,,15.64
```

```
MPDATA,CTEX,2,,16.30
MPDATA,CTEX,2,,16.94
MPDATA,CTEX,2,,17.51
MPDATA,CTEX,2,,17.99
MPTEMP,,,,,,,,
MPTEMP,1,773.15
MPTEMP,2,1173.15
MPDATA,KXX,2,,21
MPDATA,KXX,2,,24
MPTEMP,,,,,,,,
MPTEMP,1,773.15
MPTEMP,2,1173.15
MPTEMP,3,1373.15
MPDATA,C,2,,628
MPDATA,C,2,,674
MPDATA,C,2,,712
MPTEMP,,,,,,,,
MPTEMP,1,773.15
MPTEMP,2,1173.2
MPTEMP,3,1373.15
MPDE,KXX,2
MPDATA,KXX,2,,21
MPDATA,KXX,2,,24
MPDATA,KXX,2,,34
TB,CREE,2,1,3,10
TBTEMP,0
TBDATA,,10E12,3,6.014E4,,,

!TGO
!------
MPTEMP,,,,,,,,
MPTEMP,1,273
MPDATA,EX,3,,360E9
MPDATA,PRXY,3,,0.25
MPTEMP,,,,,,,,
MPTEMP,1,0
MPDE,EX,3
MPDE,PRXY,3
MPDATA,EX,3,,3.6E+011
MPDATA,PRXY,3,,0.25
MPTEMP,,,,,,,,
MPTEMP,1,0
MPDE,EX,3
MPDE,PRXY,3
MPDATA,EX,3,,3.6E+011
MPDATA,PRXY,3,,0.25
MPTEMP,,,,,,,,
MPTEMP,1,0
MPDATA,DENS,3,,3970
MPTEMP,,,,,,,,
MPTEMP,1,0
UIMP,3,REFT,,,273
MPDATA,CTEX,3,,8.00
MPTEMP,,,,,,,,
MPTEMP,1,0
MPDATA,C,3,,790
TB,CREE,3,1,3,10
TBTEMP,0
TBDATA,,6.8E3,1,5.1E4,,,
MPDATA,KXX,3,,20

!YSZ
!------
MPTEMP,,,,,,,,
MPTEMP,1,0
MPDATA,EX,4,,50E9
MPDATA,PRXY,4,,0.25
MPTEMP,,,,,,,,
MPTEMP,1,0
MPDATA,DENS,4,,5100
MPTEMP,,,,,,,,
MPTEMP,1,273
MPTEMP,2,773.15
MPTEMP,3,1273.15
UIMP,4,REFT,,,273
MPDATA,CTEX,4,,10.00
MPDATA,CTEX,4,,9.64
MPDATA,CTEX,4,,10.34
MPTEMP,,,,,,,,
MPTEMP,1,0
MPDATA,KXX,4,,0.70
MPTEMP,,,,,,,,
MPTEMP,1,273
MPTEMP,2,773.15
MPTEMP,3,1273.15
MPDATA,C,4,,479
MPDATA,C,4,,445
```

```
TB,CREE,4,1,3,10
TBTEMP,0
TBDATA,,10E10,4,7.517E4,,,
!------------Create Section ----------------------
/REPLO
sect,234,shell,,TBC
secdata, 0.00015,2,0,3
secdata, 3e-006,3,0,3
secdata, 0.0005,4,0,3
secoffset,BOT
seccontrol,0,0,0, 0, 1, 1, 1
APLOT
sect,234,shell,,TBC
secdata, 0.00015,2,0,3
secdata, 3e-006,3,0,3
secdata, 0.0005,4,0,3
secoffset,TOP
seccontrol,0,0,0, 0, 1, 1, 1
amesh,234
sect,234,shell,,TBC
secdata, 0.00015,2,0,3
secdata, 3e-006,3,0,3
secdata, 0.0005,4,0,3
secoffset,MID
seccontrol,0,0,0, 0, 1, 1, 1

!------------Change Physics ----------------------

PHYSICS,WRITE,thermal, , ,
PHYSICS,CLEAR
ETCHG,TTS
mat,1
!Insert Material properties as shown above
PHYSICS,WRITE,struc, , ,
PHYSICS,CLEAR

/COM, CONTACT PAIR CREATION - START
CM,_NODECM,NODE
CM,_ELEMCM,ELEM
CM,_KPCM,KP
CM,_LINECM,LINE
CM,_AREACM,AREA
CM,_VOLUCM,VOLU
/GSAV,cwz,gsav,,temp
MP,MU,1,
MAT,1
MP,EMIS,1,
R,3
REAL,3
ET,3,170
ET,4,174
R,3,,,1.0,0.1,0,
RMORE,,,1.0E20,0.0,1.0,
RMORE,0.0,0,1.0,,1.0,0.5
RMORE,0,1.0,1.0,0.0,,1.0
KEYOPT,4,4,2
KEYOPT,4,5,0
KEYOPT,4,7,0
KEYOPT,4,8,0
KEYOPT,4,9,0
KEYOPT,4,10,2
KEYOPT,4,11,1
KEYOPT,4,12,5
KEYOPT,4,2,2
KEYOPT,3,5,4
KEYOPT,4,1,2
! Generate the target surface
ASEL,S,,,2
CM,_TARGET,AREA
TYPE,3
NSLA,S,1
ESLN,S,0
ESLL,U
ESEL,U,ENAME,,188,189
NSLE,A,CT2
ESURF
CMSEL,S,_ELEMCM
! Generate the contact surface
ASEL,S,,,7
CM,_CONTACT,AREA
TYPE,4
NSLA,S,1
ESLN,S,0
NSLE,A,CT2 ! CZMESH patch (fsk qt-40109
8/2008)
ESURF
```

```
*SET,_REALID,3
ALLSEL
ESEL,ALL
ESEL,S,TYPE,,3
ESEL,A,TYPE,,4
ESEL,R,REAL,,3
/PSYMB,ESYS,1
/PNUM,TYPE,1
/NUM,1
EPLOT
ESEL,ALL
ESEL,S,TYPE,,3
ESEL,A,TYPE,,4
ESEL,R,REAL,,3
CMSEL,A,_NODECM
CMDEL,_NODECM
CMSEL,A,_ELEMCM
CMDEL,_ELEMCM
CMSEL,S,_KPCM
CMDEL,_KPCM
CMSEL,S,_LINECM
CMDEL,_LINECM
CMSEL,S,_AREACM
CMDEL,_AREACM
CMSEL,S,_VOLUCM
CMDEL,_VOLUCM
/GRES,cwz,gsav
CMDEL,_TARGET
CMDEL,_CONTACT
/COM, CONTACT PAIR CREATION – END
```

```
!-------------------solution part---------------------
! Start Thermal Analysis

/PREP7
PHYSICS,READ,THERMAL
FINISH
/SOL
PHYSICS,READ,THERMAL
!Define heat Flux = 0
!Define heat convection

SFA,P51X,1,CONV,3000,800

! static solution
/solu
allsel
solcontrol,on
rescontrol,,all,last,1
rate, off
delt,2.0e-8,1.0e-9,2.0e-8
time, 2.0e-8
!EQSLV,front
EQSLV,PCG,1E-8
solve


!Start structural analysis
PHYSICS,CLEAR
PHYSICS,READ,STRUC
LDREAD,TEMP,,,, , ,'layer800_update','rth','
!Apply displacement constraint

! static solution
/solu
allsel
solcontrol,on
rescontrol,,all,last,1
rate, off
delt,2.0e-8,1.0e-9,2.0e-8
time, 2.0e-8
!EQSLV,front
EQSLV,PCG,1E-8
solve
```

```
!Rate Solution (restart)
antyp,,rest,1,1
solcontrol,on
rate, on
neqit,10
delt,0.25,1e-9,5.0
time,24.0
solve



!-----------------view angle-------------------------------
!For general post processing

/VIEW,1,,-1
/ANG,1
/REP,FAST
/AUTO,1
/REP,FAST

/ZOOM,1,SCRN,0.323713,0.741848,0.125838,0.7
53261

/ANG,1,30,YS,1
/REP,FAST

/REP,FAST
/VIEW,  1, -0.244598432585    , -0.657224101439
   ,  0.712901176367
/ANG,   1,   34.2994532793
/REPLO
/VIEW,  1, -0.220386199483    , -0.549338069395
,
  0.806013404721
/ANG,   1,   31.7989066865
/REPLO


!----------------------------End-----------------------------
```

BIBLIOGRAPHY

[1] Gleeson, B., *Thermal Barrier Coatings for Aeroengine Applications*, Journal of Propulsion and Power, 2006, Vol. 22, No 2.

[2] Echsler, H., Renusch, D., Schutze, M., *Bond Coat Oxidation and its Significance for Life Expectancy of Thermal Barrier Coating Systems*, Material Science and Technology, 2004, Vol. 20, pp. 307-318.

[3] Busso, E.P., Lin J., Sakurai, S., Nakayama, M., *A Mechanistic Study of Oxidation-Induced Degradation in a Plasma-Sprayed Thermal Barrier Coating System*. *Part I: Model Formulation*, Acta Mater, 2001;49:1515-1528.

[4] Busso, E.P., Lin, J., Sakurai, S., Nakayama, M., *A Mechanistic Study of Oxidation-Induced Degradation in a Plasma-Sprayed Thermal Barrier Coating System*. *Part II: Life Prediction Model*, Acta Mater 2001;49/9:1529-1536.

[5] Busso, E.P., Qian, Z.Q., *A Mechanistic Study of Microcracking in Transversely Isotropic Ceramic-Metal Systems*, Acta Mater 2006;52:325-338.

[6] Busso, E.P., Wright, L., Evans, H.E., McCartney, L.N., Saunders, S.R.J., Osgerby, S., Nunn, J., *A Physics-Based Life Prediction Methodology for Thermal Barrier Coating Systems*. Acta Mater 2007:55:1491-503.

[7] Busso, E.P. *Oxidation-Induced Stresses in Ceramic-Metal Interfaces*. J. Phys. IV. France 9, 1999.

[8] He, M.Y., Hutchinson, J.W., Evans, A.G., *Simulation of Stresses and Delamination in a Plasma-Sprayed Thermal Barrier System upon Thermal Cycling*, Master Sci. Eng. A 2003;345:172-8.

[9] He, M.Y., Hutchinson, J.W., Evans, A.G., *Mechanics-Based Scaling Laws for The Durability of Thermal Barrier Coatings,* Materials Science 45 2001:46:249-71.

[10] Limarga, A. M., VaBen, R., and Clarke, D.R., *Stress Distributions in Plasma-Sprayed Thermal barrier Coatings Under Thermal Cycling in a Temperature Gradient*, Journal of Applied Mechanics. Vol. 78, January 2011.

[11] Karaivanov, V., *Lifetime Prediction Modeling Of Airfoils For Advanced Power Generation*, PhD Thesis, University of Pittsburgh, 2009.

[12] Brodin, H., Jinnestrand, M., Johannssin, S., and Sjostrom, S., *Thermal Barrier Coating Fatigue Life Assessment*, Siemens Publication.

[13] Wang, J.S. and Evans, A.G. *Measurement and Analysis of Buckling and Buckle Propagation in Compressed Oxide Layers on Superalloy Substrates*, Acta Mater, V. 46 (1998), pp.4993-5005.

[14] Budianski, B. and Wu, T. *Theoretical of Plastic Strain in Polycrystals*, Proc. 4th US Nat. Congr. Appl. Mech., 1962, p. 1175.

[15] Mucke, R. *A Viscoplastic Modeling Approach or MCrAlY Protective Coatings for Gas Turbine Applications*, Baden Switzerland.

[16] Ahrens, M., Lampenscherf, S., Vassen, R., and Stover, D., *Sintering and Creep Processes in Plasma-Sprayed TBCs*, J. Thermal Spray Technology, 2004, 13 pp. 432-442.

[17] Schwarzer, J., and Vohringer, O., *High Temperature Deformation Behavior of the Bondcoat Alloy PWA 1370*, Advanced Engineering Material, 2003, pp. 490-493.

[18] Brindley, W. J., and Whittenberger, J. D., *Stress Relaxation of Low Pressure Plasma-Sprayed NiCrAlY Alloy*, Material Science Engineering A, 1993, 163, pp. 33-41.

[19] Demasi, J. T., Sheffler, K. D., and Ortiz, M., *Thermal Barrier Coating Life Prediction Model Development*, NASA Technical Report No. 182230, Cleveland, OH, 1989.

[20] Bednarz, P., *Finite Element Simulation of Stress Evolution in Thermal Barrier Coating Systems*, Ph.D. Thesis, Forschungszentrum Jülich GesmbH, Jülich, 2006.

[21] Busso, E. P., Qian, Z. Q., Taylor, M.P., and Evans, H. E., *The Influence of Bondcoat and Topcoat Mechanical Properties on Stress Development in Thermal Barrier Coating Systems*, Acta Mater., 2009, Vol. 57, pp. 2349-2361.

[22] VaBen, R., Kerkhoff, G., and Stover, D., 2001, *Development of Micromechanical Life Prediction Model for Plasma Sprayed Thermal Barrier Coating*, Material Science Engineering A, 303, pp. 100-109.

[23] Nelson, T. and Wang E., *Reliable FE-Modeling with ANSYS*, CADFEM GesmbH, Munich, Germany.

[24] Zaretsky, E. V., Litt, J.S., Hendricks R.C., *Determination of Turbine Blade Life from Engine Field Data,* NASA Glenn Research Center, Cleveland.

[25] Manet, V., *The Use of Ansys To Calculate Sandwich Structures*, Composites Science and Technology 58, 12 (1998) 1899-1905, hal-00659205, Ver. 1 – 26.

[26] Johnson, D. H., *Principles of Simulating Contact Between Parts using ANSYS*, Penn State–Erie University, Erie, Pennsylvania.

[27] Metrisin, J. T., *Guidelines for Obtaining Contact Convergence*, Turbomachinery, Florida Turbine Technologis Inc. 2008 International ANSYS Conference.

[28] *Anisotropic Behavior Yield Criterion Failure Criteria*, Review of Yield/Failure Criteria, ANSYS Newsletter.

[29] Hsueh, C. H., and Fuller, E.R., *Analytical Modeling Of Oxide Thickness Effects On Residual Stresses In Thermal Barrier Coatings*, Oak Ridge National Laboratory, Oak Ridge, Tennessee 37831-6068 National Institute of Standards and Technology, Gaithersburg, Maryland 2008.

[30] Nitin, P., Padture, et al. *Thermal Barrier Coatings for Gas-Turbine Engine Applications, Science* 2002:296.